Technical Report No. 32-146

# Experimental Studies of Unstable Combustion in Solid-Propellant Rocket Motors

E. M. Landsbaum

F. W. Spaid



jpl
JET PROPULSION LABORATORY
CALIFORNIA INSTITUTE OF TECHNOLOGY
PASADENA, CALIFORNIA

August 4, 1961

NATIONAL AERONAUTICS AND SPACE ADMINISTRATION
CONTRACT NO. NASW-6

*Technical Report No. 32-146*

# *Experimental Studies of Unstable Combustion in Solid-Propellant Rocket Motors*

*E. M. Landsbaum*
*F. W. Spaid*

Leonard R. Piasecki

Leonard R. Piasecki, *Chief*
*Solid Propellant Engineering Section*

JET PROPULSION LABORATORY
CALIFORNIA INSTITUTE OF TECHNOLOGY
PASADENA, CALIFORNIA

August 4, 1961

# CONTENTS



# FIGURES

## FIGURES (Cont'd)

## ABSTRACT

Studies have been continued of combustion instability in tubular, case-bonded solid-propellant rocket motors using polysulfide–ammonium perchlorate propellants. Early studies showed a correlation between the delay time from ignition to onset of instability and initial chamber pressure at high initial grain temperature: The lower-temperature data, reported here, showed a poor correlation. Although two experiments were conducted to study delay time, this phenomenon is still unexplained. Previous studies also showed, for a given motor geometry and grain temperature, that intensity of instability is a function of initial chamber pressure. This Report demonstrates that these trends apply to a wider range of grain dimensions and temperatures. Regions of strong instability, weak instability, and stable operation have been mapped out in the pressure–grain temperature plane for various motor configurations. Web thickness has been shown to affect instability. Measurements indicated that strong pressure waves had been transmitted through the propellant grain.

Three modifications were prepared of the propellant which was used in the majority of the experiments. The propellant in which the burning-rate catalyst and oxidizer grind were changed showed stable operations over a wide pressure range. Another propellant, in which the major change was an increase in oxidizer loading, exhibited severe instability over a much wider range.

Several experiments were conducted in which hollow chambers were attached at either the head or nozzle end of the propellant grains. The results indicated neither a frequency-selective nor viscous damping effect but indicated that instability associated with oscillations in the fundamental tangential mode is independent of longitudinal modes. It was noted that motors which showed severe instability exerted reasonably large torques about their longitudinal axes. The origin and implications of these torques are discussed. Increases in burning rate have been correlated with high-frequency pressure oscillation amplitudes, and the data appear to be in agreement with an erosive-burning mechanism.

# I. INTRODUCTION

The earliest attempts to eliminate combustion instability in solid-propellant rocket motors were usually such devices as the cutting of slots or holes in a grain and the use of a "resonance rod," a metal rod installed in the axial perforation of the grain. These methods, however, tended to reduce the performance of a motor by reducing its volumetric loading of propellant and its mass ratio. Propellant additives, in most applications, have proven to be a better means of eliminating combustion instability, but the addition of an instability-suppressing additive to a propellant after a propellant-motor system is in an advanced development stage often necessitates costly design changes. As the solid-propellant industry develops increasingly larger motors, the advantages in cost and development time of being able to predict and control combustion instability becomes increasingly obvious.

At the time (1957) that the program described here was initiated, experimental work on combustion instability had been limited primarily to attempts at finding resonance "fixes" for particular motors. It was decided that a body of data obtained from carefully controlled experiments, in which motor-design parameters were varied systematically, would be useful in testing theoretical analyses of the problem and could lead to an empirical method for the prediction of instability. These considerations led to the planning of a three-phase program. Phase I is a determination of the important experimental variables and a delineation of regions of stability and instability by the use of a single propellant in a simple configuration. Phase II is an extension of Phase I to more complex grain designs. Phase III used a variation of propellant properties. Phase I has been completed and the results are described in this Report and in Refs. 1 through 3. Reference 3 includes a theoretical study based on a time-lag concept. In Phase II, experiments were conducted with a number of similar star grains; the results will be published in a separate Report.

# II. DESCRIPTION OF EXPERIMENTS

In the experiments described here, a simple tubular shape grain was used because the acoustic properties of the cylindrical cavity are well understood and it is reasonably related to motors in production. These case-bonded, end-restricted, solid-propellant grains are referred to by the numbers $3 \times 5 \times 38$, et cetera, which are, respectively, the nominal initial port diameter, the inner-case diameter, and the grain length (dimensions in inches). The motor cases and nozzles used were heavy hardware designed for continual re-use (Fig. 1). The majority of the combustion tests used a polysulfide–ammonium perchlorate propellant of medium impulse ($c^* = 4236$ ft per sec at 160°F) which was designated Propellant A. Burning-rate relations for this propellant are given in Fig. 2. Reference 4 includes a detailed discussion of the instrumentation.

The initial combustion-instability studies (Refs. 1 and 2) were concerned with the interaction of pressure and frequency and, to a lesser degree, the effect of temperature. Demonstrating that unstable combustion was, like many other phenomena, reproducible and that it varied systematically with its controlling parameters was a major accomplishment. The division of the pressure-frequency plane into regions of unstable and stable combustion was another major finding. The unstable region could be further divided into weak and strong unstable zones, and the boundaries of these regions were temperature dependent. In the strongly unstable region, the degree of instability increased with increasing initial chamber pressure. When the weakly unstable region was reached, the degree of instability decreased sharply, and at still higher pressures the firings became completely stable. These experiments have been extended to other temperatures and grain sizes with similar results.

The majority of the earlier investigations was made at 160°F, at which temperature the delay time from ignition to instability showed a correlation with the initial chamber pressure. It was later determined that, at other temperatures, any relation appears random. This delay time was unaffected by pre-pressurizing the rocket motor or insulating the metal components.

The effects of web thickness on instability were examined. Measurements of the pressure oscillation in the grain made at the interface of grain and case gave very high values. The results indicate that the gas–solid acous-

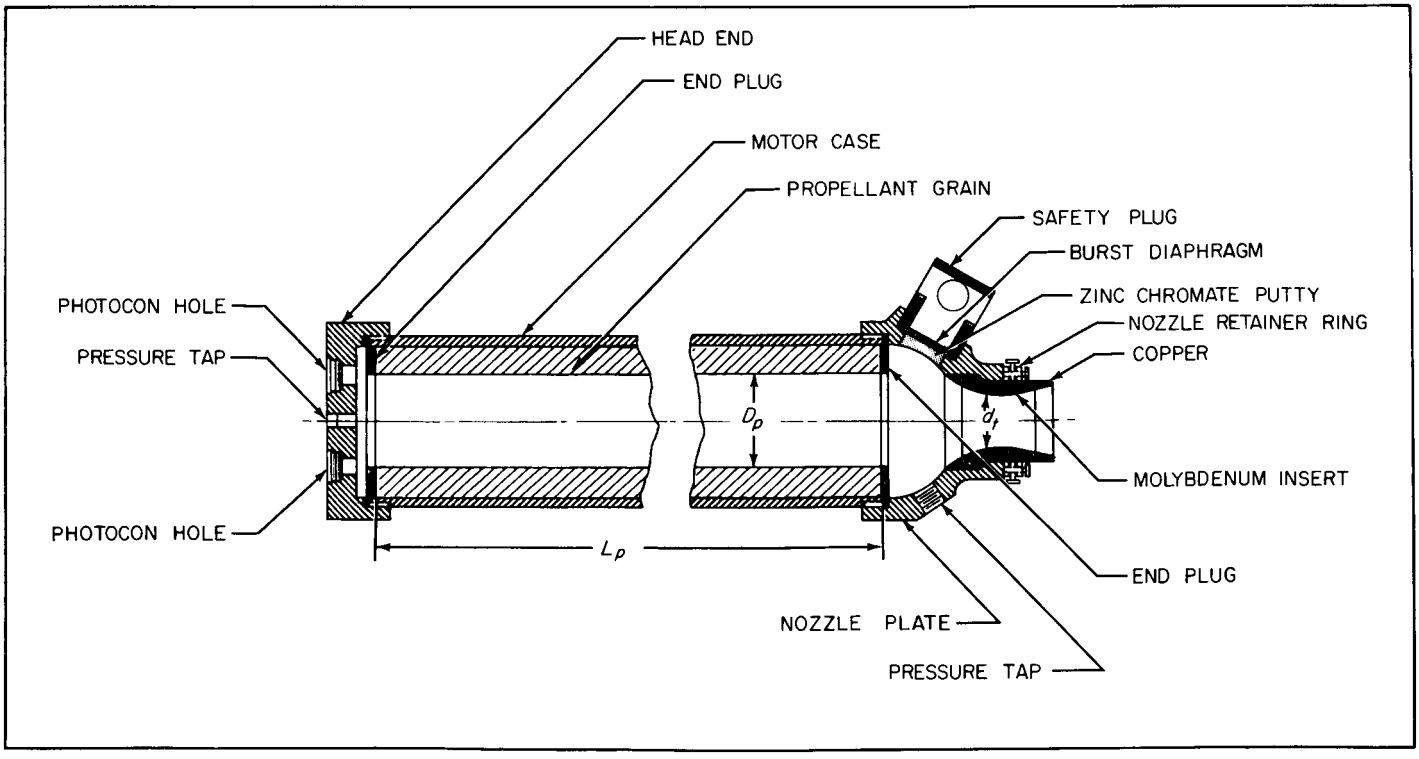


**Fig. 1. Sectioned view of a tubular motor**

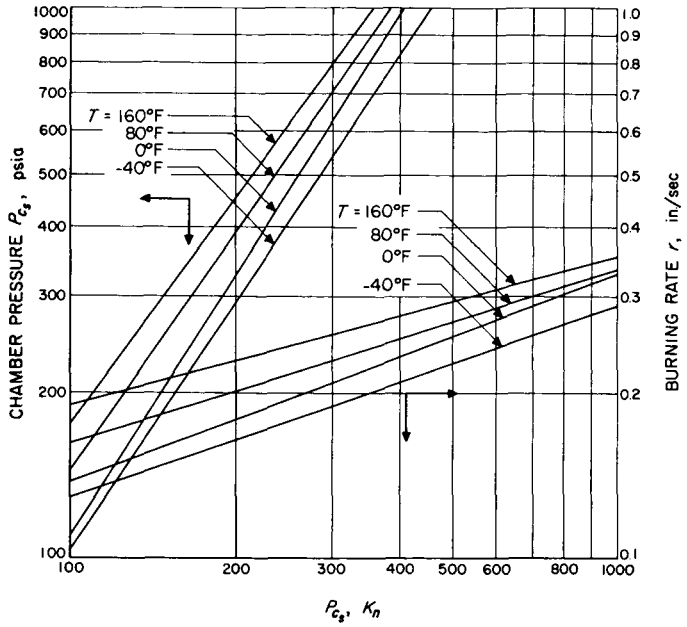


**Fig. 2. Burning-rate relations, Propellant A**

tic interaction cannot be predicted on the basis of simple acoustic theory.

In one of the propellant modifications, a change in the burning-rate catalyst and oxidizer grind produced stable combustion over the wide pressure range investigated. Two motors with carbon black added and fired near the point of maximum instability also gave stable burning. The third modification, an increase in oxidizer loading, resulted in an increased pressure range in which unstable burning was observed.

In several motor firings, hollow chambers of various lengths were added at either the head end or nozzle end of the motors. Instability was practically unaffected by the head-end chambers, but it was either greatly decreased or completely eliminated by any one of the nozzle-end chambers.

The burning-rate increases during periods of unstable combustion were examined, and it is shown here that an erosive-burning mechanism gives a reasonable explanation of these increases.

## III. EXPERIMENTAL RESULTS

Results of the determination of experimental variables and the delineation of stable and unstable regions for a simple configuration using a single propellant are presented.

### A. Delay Time from Ignition to Instability

The delay time from ignition to instability presents a rather puzzling problem. Results from a great number of motor firings are presented in Fig. 3. The initial port diameter ($D_{p_i}$ = 4 in.) data are new; the other data are from Ref. 1. It has been shown previously that the delay time did not represent a period in which the instability was prohibited by an improper relationship between frequency and pressure. Neither could it be attributed to a composition difference in the initial layer of propellant.

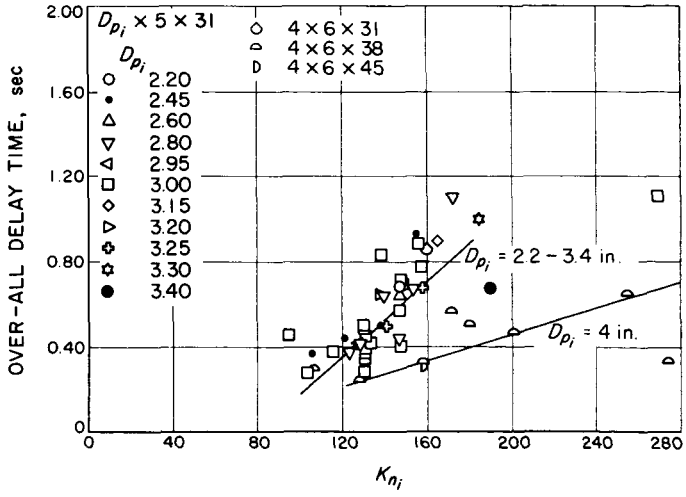


**Fig. 3. Delay time vs $K_{n_i}$ at 160°F**

The delay time shows an increase with web thickness and pressure and a decrease with initial perforation diameter, indicating a possible relation to the physical properties of the propellant. At lower temperatures, however, as shown in Fig. 4, the delay time appears more random and less correlated and the propellant modulus is higher.

The propellant is a visco-elastic material, and it was believed that a correlation might exist between the delay time from ignition to onset of instability and the time required for the propellant strain rate to decrease to some sufficiently small value after the sudden loading of the grain caused by ignition. A test was conducted in which two $3 \times 5 \times 38$ motors were fired at an initial burning area–throat area ratio ($K_n$) of 135 and an initial grain temperature of 80°F. The first motor was fired without a nozzle closure; the grain was exposed to atmospheric pressure prior to ignition. The second motor had a lucite diaphragm installed slightly forward of the throat. This motor was pressurized with dry nitrogen to its initial operating pressure of 265 psia before firing. The pressure–time curves for both motors are shown in Fig. 5. The small effect on the delay time was considered to be within the usual scatter of delay-time data.

One other possible explanation of the delay time is the time required for the motor parts to heat sufficiently not to represent too much of a dissipative mechanism. An experiment was conducted to test this theory in which two nearly identical motors were fired; one motor had head and nozzle plates which were insulated with fiberglass, whereas, the other motor was fired with the usual bare metal head and nozzle plates. The difference in delay time of these firings was not considered to be significant. An adequate explanation of the delay-time phenomenon is still required.

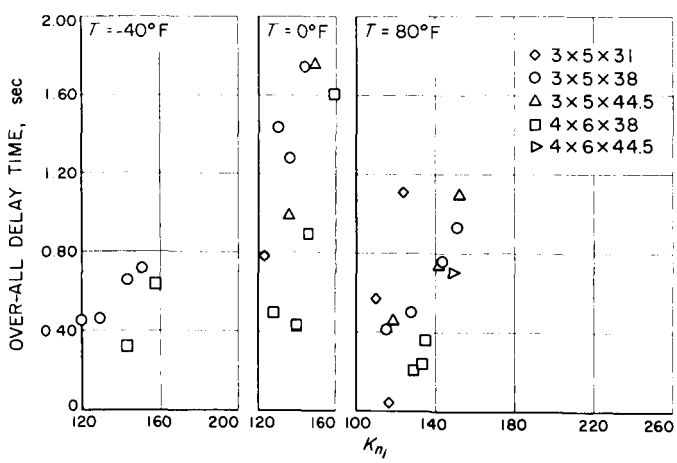


**Fig. 4. Delay time vs $K_{n_i}$ at −40, 0, and 80°F**

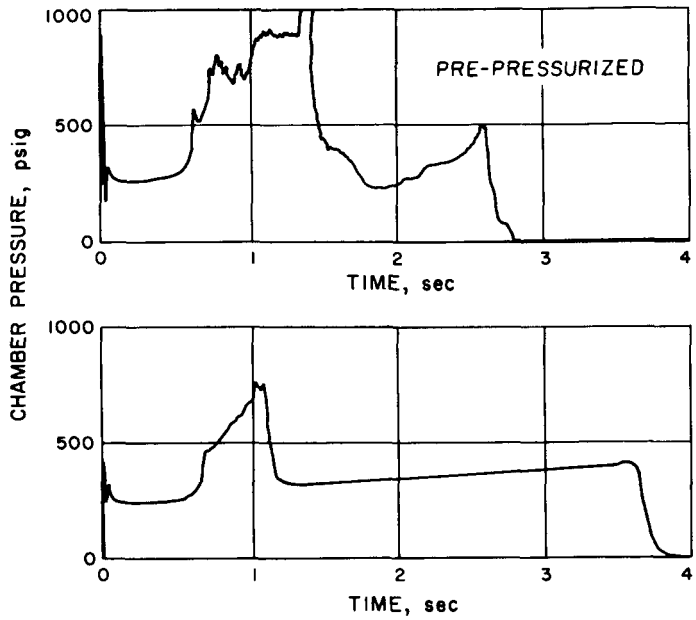


**Fig. 5. Effect of pre-pressurization on delay time; motors $3 \times 5 \times 38$ at 80°F, $K_{n_i} = 135$**

### B. Effect of Initial $K_n$ on Instability Level

The results presented here (Figs. 6 through 13) for motors fired at several initial grain temperatures and with several different grain geometries show the same trends which were reported in Ref. 1 for motors fired only at 160°F. The dependent variable here is instability level, which is defined as follows:

$$\text{instability level} = \frac{\Delta \overline{P}_c}{P_{c_s}} = \frac{\overline{P}_{c_b} - P_{c_s}}{P_{c_s}} \qquad (1)$$

where $P_{c_b}$ is the actual mean chamber pressure of the "break" point, and $P_{c_s}$ is the stable chamber pressure that should have existed at that value of $K_n$. This quantity was computed at the initial "break" point of each pressure–time curve, that is, the point after the onset of instability at which an abrupt decrease in the slope of the curve was observed. (Instability level is discussed in greater detail in Ref. 1.)

The firings show a linear increase of instability level with $K_{n_i}$ over the range covered. The slope of this line does not appear to be independent of motor size and temperature. Also, it is better defined for those combinations of initial grain temperature and grain geometry which have high values of maximum instability level than it is for those combinations which have only a moderate maximum instability level. The increase in instability level

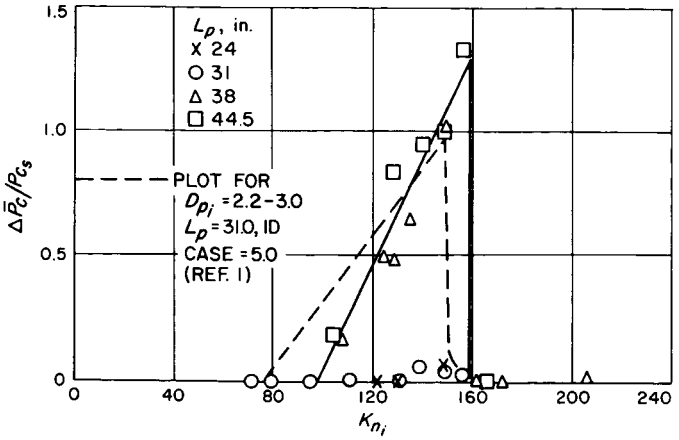


**Fig. 6. Instability level vs $K_{n_i}$; motors 3 × 5 × 24, 31, 38, and 44.5 at 160°F**

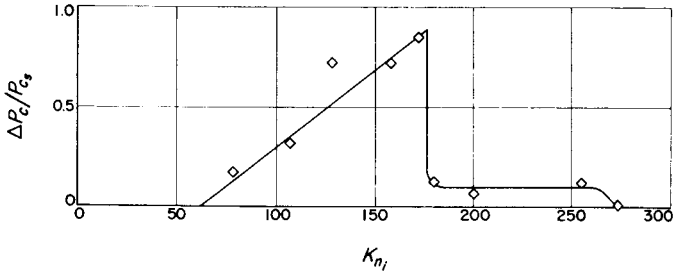


**Fig. 7. Instability level vs $K_{n_i}$; motors 4 × 6 × 38 at 160°F**

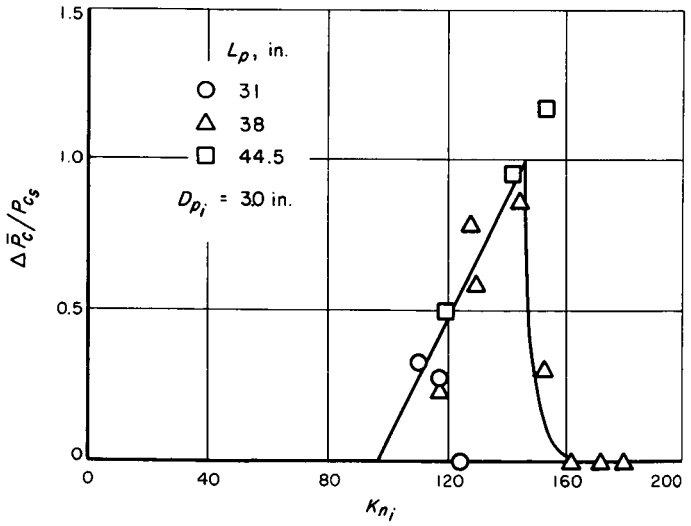


**Fig. 8. Instability level vs $K_{n_i}$; motors 3 × 5 × 31, 38, and 44.5 at 80°F**

continues only until the value of $K_n$, henceforth called $K_{n_{max}}$, is reached; a further increase in $K_n$ above $K_{n_{max}}$ yields a rapid decrease in the instability level. Further increases of $K_{n_i}$ yield no instabilities above some point, henceforth called $K_{n_s}$, and here stable burning is reached. Very few 4 × 6 × 38 motors were fired at values of $K_n$ below $K_{n_{max}}$ or above $K_{n_s}$ at temperatures other than

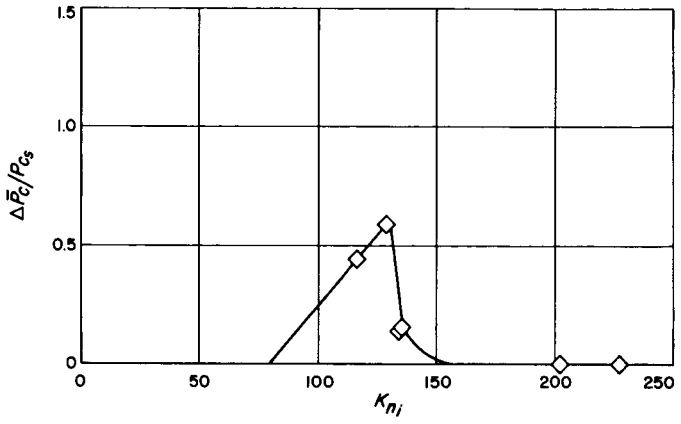


**Fig. 9. Instability level vs $K_{n_i}$; motors 4 × 6 × 38 at 80°F**

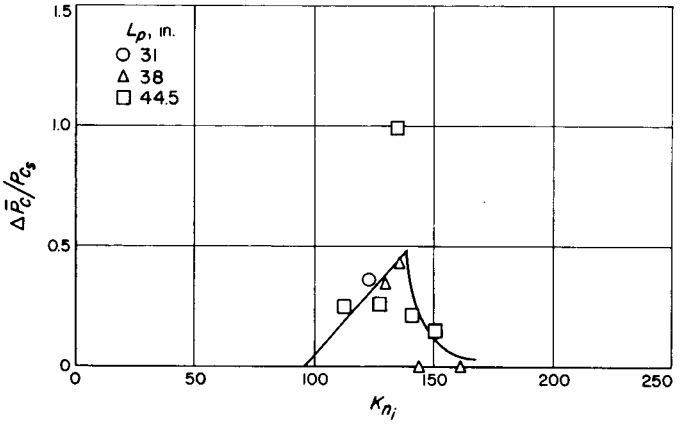


**Fig. 10. Instability level vs $K_{n_i}$; motors 3 × 5 × 31, 38, and 44.5 at 0°F**

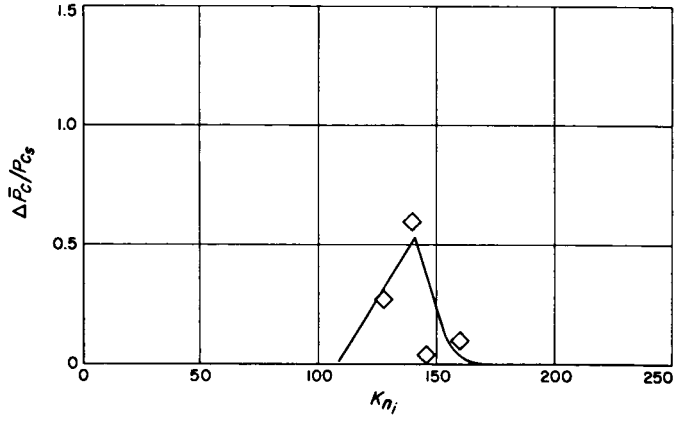


**Fig. 11. Instability level vs $K_{n_i}$; motors 4 × 6 × 38 at 0°F**

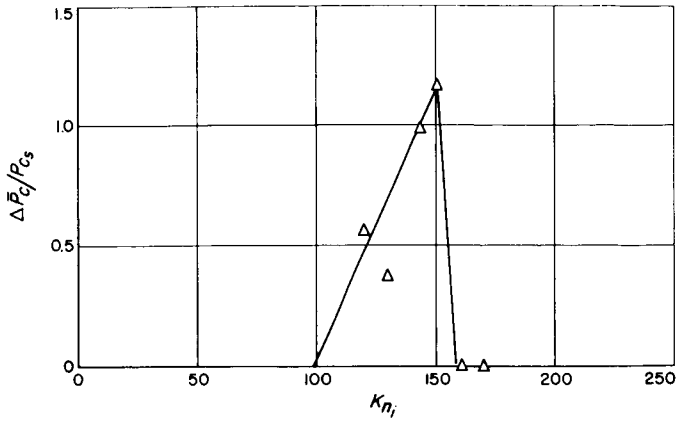


**Fig. 12. Instability level vs $K_{n_i}$; motors 3 × 5 × 33 at −40°F**

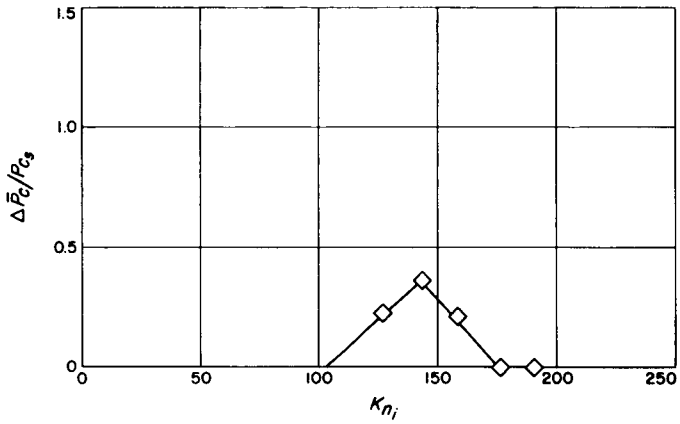


**Fig. 13. Instability level vs $K_{n_i}$; motors 4 × 6 × 38 at −40°F**

160°F. However, the data which have been accumulated at these conditions do agree with the more extensive data taken at 160°F, and at the other temperatures with 3 × 5 × 31, 38, and 45 motors, in that definite values of $K_{n_{max}}$ and $K_{n_s}$ were found for each case.

Figure 6 shows data from Ref. 1 on 2.2-3.0 × 5 × 31 motors and also shows more recent data which were obtained from 3 × 5 × 31 motors. It can be seen that the values of $K_{n_{max}}$ for each set of data are very nearly the same, but the values of instability level for the later data are very much lower than had previously been measured. The instability levels measured for 3 × 5 × 38 motor firings can be seen to agree very well with the earlier data. One possible interpretation of these findings is as follows: For a motor of a given port diameter, web, and initial grain temperature, there is a critical grain length, or $L/D$, below which little or no instability will be observed, regardless of chamber pressure, and above which strong instability will be observed at some range of chamber pressures. This critical length appears to be affected by small changes in propellant composition caused by lot-to-lot variations in raw materials. The length of 31 in. for this particular motor configuration and initial grain temperature appears to be very nearly critical, therefore changes in raw materials have been sufficient to have caused the observed reduction in instability level between the early and later firings. The 38 in. length appears to have been sufficiently greater than the critical length that it was not affected by the material lot changes. The earlier data from 31-in. length motors are consistent with the data taken from firings of longer motors. It appears, therefore, that the use of this length motor was justified at the time and that these firings produced useful data.

The plots of instability level versus $K_{n_i}$ suggest that a second region of stable operation might be reached by firing motors at sufficiently low values of $K_{n_i}$. Figure 14 shows pressure–time curves obtained from two 4 × 6 × 38 motors which were fired at relatively low values of $K_{n_i}$. It can be seen that a new region of stable operation has not been found, but the instability level has reached a low level, particularly in the case of the firing at a $K_{n_i}$ of 68. The trend of increasing delay time with increasing pressure appears to have been reversed at these low pressures and these motors exhibit very long delay times compared with the delay times of the other firings, as can be seen in Fig. 6.

It would be desirable to fire motors at lower values of $K_n$, but doing this presents practical problems. Previous results indicate that a sufficiently large $L/D$ must be maintained if severe instability is to occur. If a constant

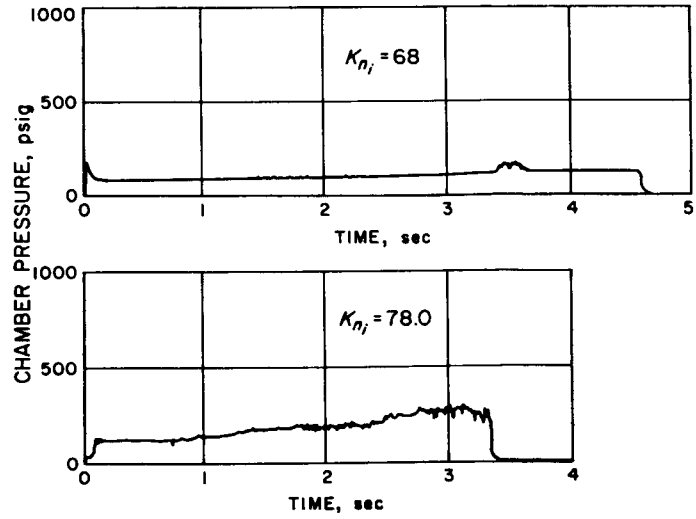


**Fig. 14. Low-pressure motors; 4 × 6 × 38 at 160°F**

$L/D$ is maintained and the $K_{n_i}$ is reduced, this amounts to increasing the nozzle throat area and allowing the port-to-throat ratio to approach unity. Very low port-to-throat ratios (near 1) result in large erosive-burning effects during the initial portion of the firing, which make interpretation of the data difficult. Motors fired at low values of $K_{n_i}$ are necessarily fired at low initial chamber pressures. Low chamber pressures are accompanied by ignition difficulties and by a tendency for the motors to chuff rather than to sustain burning after ignition. These problems are aggravated if the grain temperature is decreased.

### C. Effect of Grain Temperature

A number of motors was fired to investigate the effect of initial grain temperature in order that $K_{n_{max}}$ and $K_{n_s}$ could be determined as a function of initial temperature. The results are presented in Fig. 15. The data on the $3 \times 5 \times 31$ motors are from Ref. 1. It had been thought, incorrectly, that the upper stability line, as defined by the $3 \times 5 \times 31$ motors, would be independent of length. The data given in Fig. 15 illustrate a well-known effect: The instability of a motor of fixed $K_n$ is usually more pronounced at the high- and low-temperature extremes. However, a high $K_n$ would have been stable throughout the temperature region, and a lower $K_n$ would have been unstable throughout the temperature region.

It can be seen that $K_{n_{max}}$ is a definite function of length or $L/D$ ratio and that $L/D$ ratio also affects $K_{n_s}$, particularly at the lower temperatures. The behavior of $4 \times 6 \times 38$ motors is consistent with the $3 \times 5 \times 31$ motors but not with the $3 \times 5 \times 38$ motors, apparently because of varying $L/D$ ratios. It also appears that the critical $L/D$ ratio may vary with temperature.

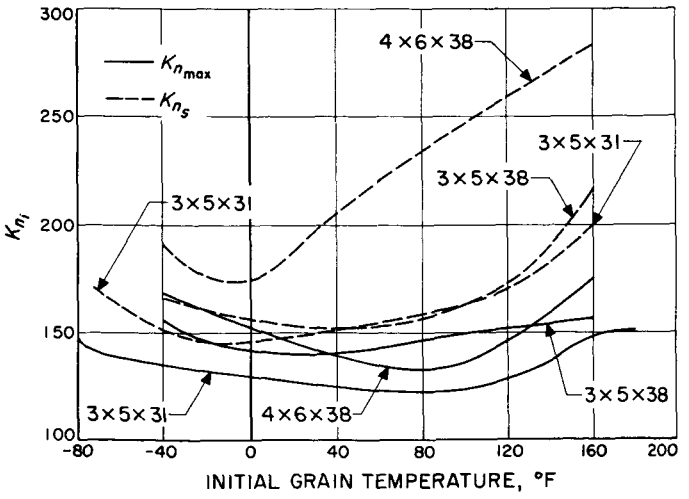


**Fig. 15. Stability limits in the $K_n$–temperature plane**

The motors are highly erosive at the lower temperatures, about 40% at −40°F, therefore, it seems appropriate to present the data of Fig. 15 on a pressure basis also. This has been done in Fig. 16. The pressures used to obtain the curve shown in Fig. 16 are the actual operating pressures at diameters of 3.15 and 4.15 in. for the $3 \times 5$ and $4 \times 6$ motors, respectively. The maximum instability level is also a function of temperature and motor size, as shown in Fig. 17. The minimum value of the maximum instability level, for $3 \times 5 \times 38$ motors, at near normal temperatures, is another explanation of more pronounced instability at high- and low-temperature extremes.

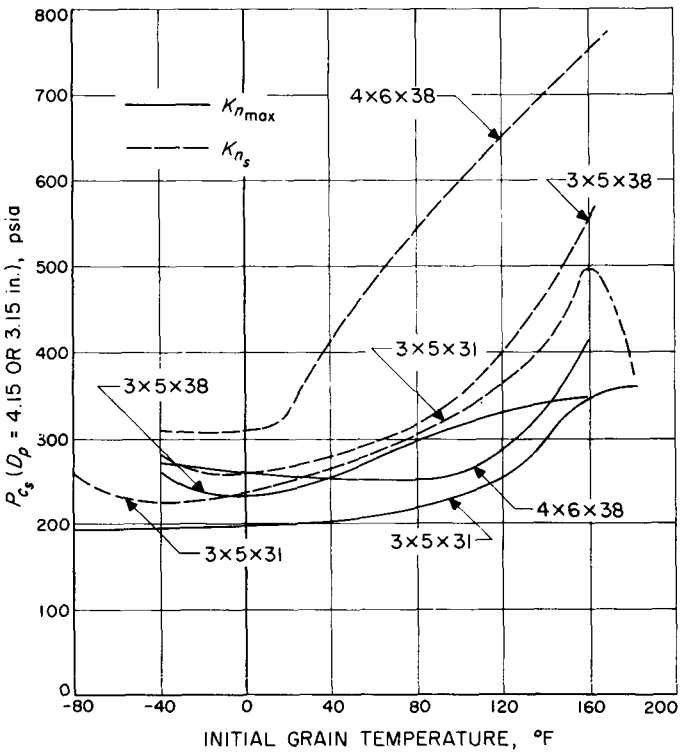


**Fig. 16. Stability limits in the pressure–temperature plane**

Figure 18 illustrates the effect of temperature on the character of maximum instability for a particular motor geometry. The character of maximum instability for the $3 \times 5 \times 31$ and the $4 \times 6 \times 38$ motors at −40°F was very similar to that of the $3 \times 5 \times 38$ motors, which were conditioned to an initial grain temperature of 0°F.

The large differences in maximum instability level among the $3 \times 5 \times 38$ motors and the motors of the two other configurations at the lower grain temperatures establishes the fact that the temperature affects the critical length or $L/D$. The changes in the actual burning rate suggest that the critical length may be related to the variation in burning rate. Because of erosive burning,

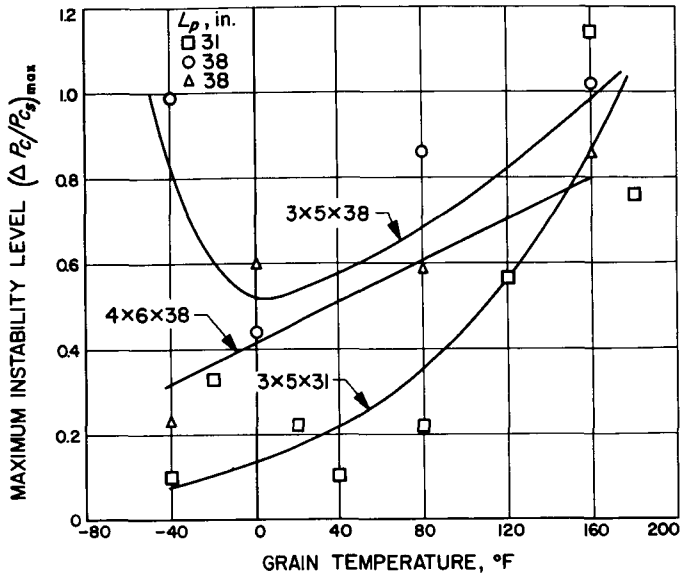


**Fig. 17. Maximum instability level vs temperature**

the pressures given in Fig. 16 are not related to $K_n$ through nonerosive data. At $K_{n_{max}}$ the $3 \times 5 \times 31$ motors at 160°F have $r = 0.3$ in. per sec and the $3 \times 5 \times 38$ motors at −40°F have $r = 0.22$ in. per sec. The former motor gives $rL = 9.5$ in.$^2$ per sec, and for the latter motor, $rL = 8.5$ in.$^2$ per sec. The parameter $rL$ is also proportional to the energy input. The losses in both motors should be approximately the same, except for the lower absorption of the low-temperature propellant, and the required energy input should also be the same. The postulated relationship between critical length and burning rate therefore seems reasonable. On an energy basis, $rL = 8.5$ in.$^2$ per sec is equivalent to 4.8 $Q$ Btu per sec, where $Q$ is the heat of combustion of the propellant.

### D. Stability Limits

A plot is presented in Ref. 1 of $K_n$ versus port diameter for motors with grain lengths of 30, 31, and 32 in., case I.D. of 5.0 in., and grain temperatures of 160°F. This plot divides the plane into regions of severe instability, weak instability, and stable operation. The boundaries of these regions are presented in Fig. 19 with data from more recent motor firings at slightly different grain lengths, case I.D., and web thicknesses. It can be seen that the data agree with the stability limits as they were originally drawn. The motor which was fired with no detectable instability at a port diameter of 5.47 in. had such a thin web that the duration of the firing was much less than the average delay time of other motors fired in that region of weak instability. The data at the lower port diameters (less than 2.5 in.) were difficult to interpret because the maximum instability levels measured here were extremely low.

### E. Effect of Web Thickness

Certain effects were noticed, primarily due to web thickness, that can probably be traced back to the propellants' physical properties. The interpretation of the results, although qualitative in nature, may be helpful in further theoretical analysis, particularly regarding dissipation mechanisms.

A number of firings illustrating the effect of web thickness and also a possible interrelationship of $L/D$ ratio are shown in Fig. 20. Firing curve (a) for a thicker web does not have the characteristic spike of the strong insta-

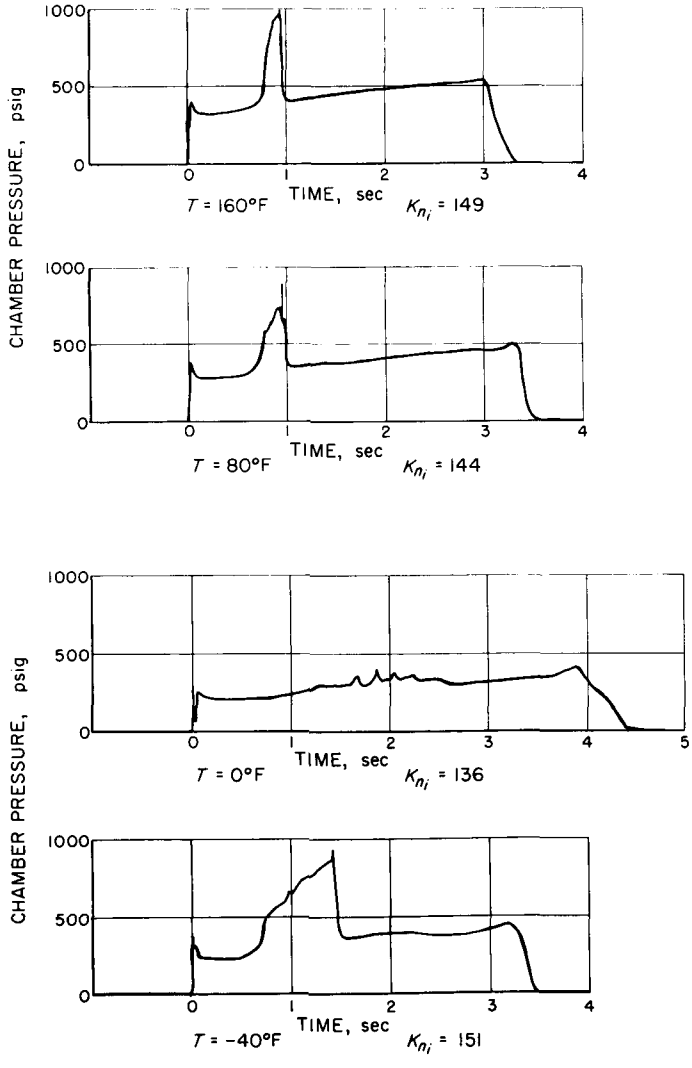


**Fig. 18. Effect of temperature on character of maximum instability for $3 \times 5 \times 38$ motors**

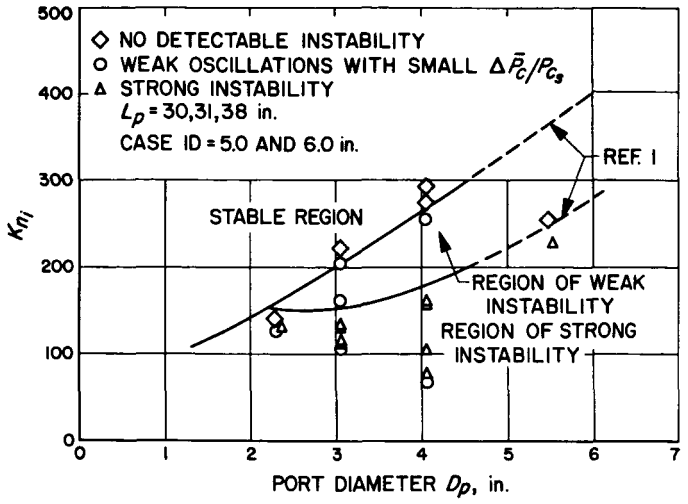


**Fig. 19. Stability limits in the $K_{n_i}$–initial port-diameter plane at 160°F**

bility region, and this appearance is characteristic of other motors in its immediate region. Yet, firing curves (b) and (c), obtained from motors fired on either side of (a), show the characteristic spike of the strongly unstable region and have thinner webs. Similarly, compare firing curve (c) and (d). Although fired under slightly different conditions, curve (d) would be expected to show the presence of instability; however, it apparently shows completely stable burning. The absence of instability can be explained by the thicker web during the early part of the run followed by entrance into the weakly unstable zone during the latter part of the run. Curve (e) showed rather wild gyrations, but the initial portion of the curve shows that (e) does not have the characteristic unstable spike noted in curve (f).

A possible interrelationship of web thickness and $L/D$ ratio is shown in firing curves (g), (h), (i), and curve (j), a shorter motor, shows apparently stable burning presumably because of the shorter length. Curve (i), however, shows an apparently typical instability occurring near the wall, and curve (j), a slightly longer motor than that of (i), shows the instability occurring early in the run.

The general agreement between (g) and (j) indicates that the effect of web thickness must be small in the range from 0.5 to 1.0 in. The relation of (g) to (h) and (j) to (i) is another example of $L/D$-ratio effects. The difference between (i) and (h) may also be an effect of the $L/D$ ratio. At burnout, (i) has a higher $L/D$ ratio than (h), and, coupled with the low absorption of the thin web, instability is possible. Although the damping effect of the web must be small at 0.5 in., it is sufficient to prevent motor (h) from becoming unstable at $D_p = 5.0$ in.

Although these observations are necessarily somewhat qualitative, there seems to be a definite influence of the web thickness and also an interaction with the $L/D$ ratio on the character of the instability. One reason for the stable behavior following the instability spikes might be $L/D$-ratio and web-thickness effects, which may also explain the large instabilities obtained with low ac pressures near burnout. Near burnout, the increase in mean pressure for ac oscillation pressure is much greater than that found at the beginning of runs.

The influence of temperature (and possibly a physical-property effect) on the character of the instability can be seen in Fig. 18. It can be noted that the 0°F firing shows an instability character similar to that shown in Fig. 20 for the large web thickness. No explanation for this behavior can be given at the present time.

A more systematic study of the effect of web thickness and propellant physical properties was attempted. Motors with 1.5 to 2.0 port diameters were fired in 3.0 I.D. cases with grain lengths from 17.0 to 29.75 in. at various pressures and at an initial grain temperature of 160°F. None of these motors exhibited a large instability level, however. The intent of this series of tests was to fire a motor of this size exhibiting severe instability and to fire similar motors in larger cases. These motors would be essentially identical except for the web thickness. If this had been accomplished, the testing would have been extended to several grain temperatures. Figure 20 indicates that $K_{n_{max}}$ decreases with decreasing port diameter. Since other findings indicate that a sufficiently large $L/D$ must be maintained, the firing of a strongly unstable motor with a port diameter of less than 2.0 in. is complicated by problems with low-pressure ignition and the sustaining of combustion, plus large erosive-burning effects.

Experiments were conducted to determine the extent of pressure oscillations through the propellant web. A $3 \times 5 \times 40$ rocket motor was assembled with provision for the installation of two Photocon pressure gauges at a distance of 18 in. from the nozzle end of the grain and 90 deg apart on the circumference of the motor case. The pressure-sensing faces of the gauge were mounted against the grain at the interface between the grain and the motor-case wall. Two additional Photocons were mounted on the headplate of the motor.

Two such motors were fired, one at 80°F and the other at −40°F. The oscillations were expected to be low in the grain and the gauges were calibrated accordingly for the first run at 80°F. As a result, the data were not useful, although high vibration levels were indicated,

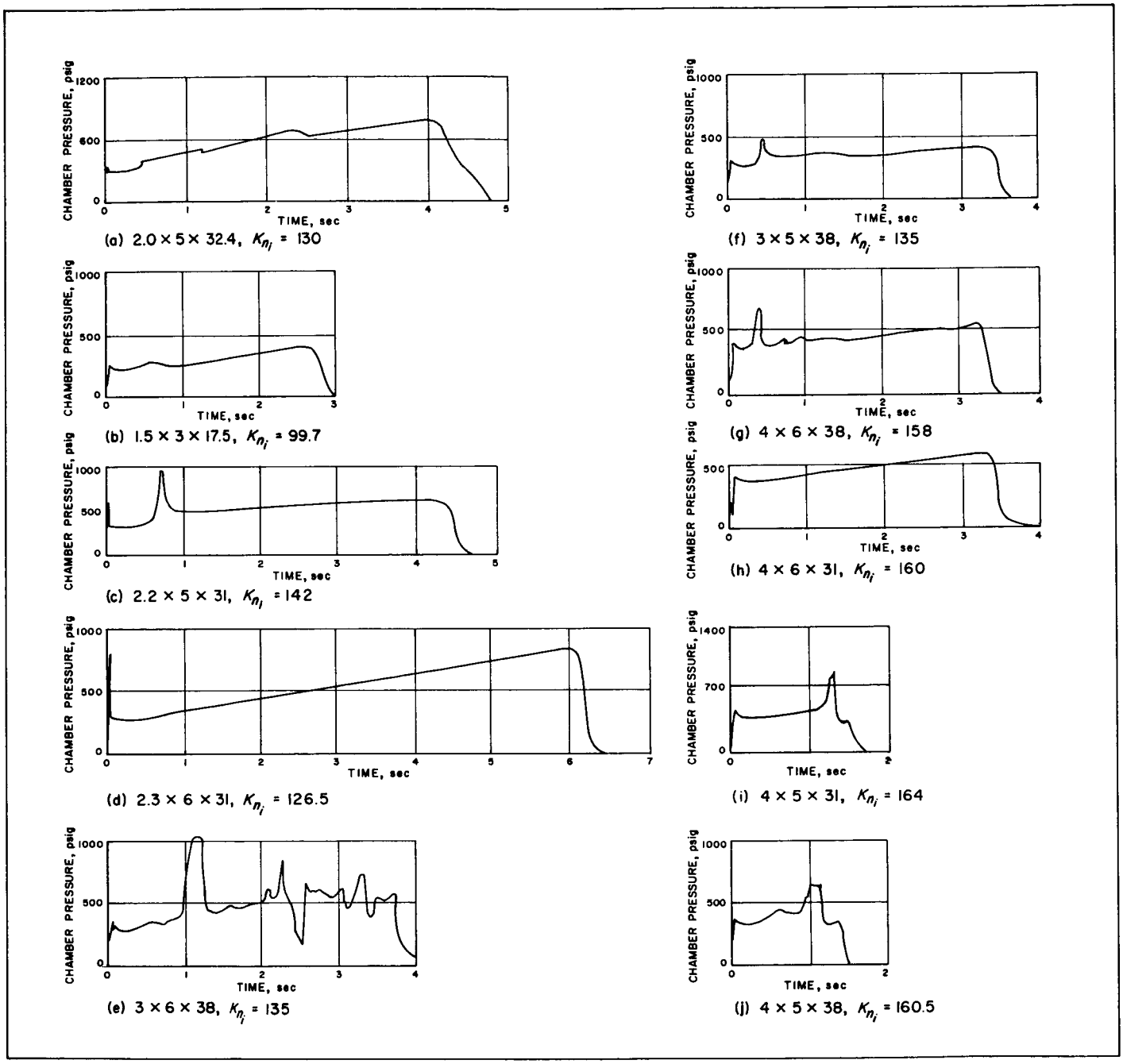


**Fig. 20. Effect of web thickness on character of instability; $T = 160°F$**

and the pressure oscillations were first detected by the side-mounted gauges, suggesting that the tangential mode of oscillation originates near the center of the grain.

The run at −40°F was more successful. Oscillations of approximately 600 psi peak-to-peak were measured with the side gauge and about 300 psi peak-to-peak with a gauge mounted in the standard head-end position. Frequency analysis indicated that the fundamental frequency was the first tangential mode, about 6 kc. The side-mounted gauge had an extremely high harmonic content, particularly the first overtone (about 12 kc) which had an amplitude equal to that of the fundamental. The analyzer is sufficiently accurate to distinguish between the first radial mode and the first overtone of the first tangential mode. However, small perturbation theory may not hold to the required accuracy of 4% at these high amplitudes. All the higher overtones were also present,

but to a lesser degree. The head-end gauge had the normal low amount of overtone but in general produced a pure sine wave.

The high-pressure oscillations existing in the propellant web are puzzling. Elementary acoustic theory indicates that the oscillations should have a much lower amplitude. Expressions have been derived for the ratios of the transmitted-to-incident amplitude and energy for a wave traveling normal to the interface between two media (Ref. 3). The amplitude ratio is:

$$t_{12} = \frac{2(\rho c)_1}{(\rho c)_1 + (\rho c)_2} \tag{2}$$

and the energy ratio is:

$$I_{12} = \frac{(\rho c)_2}{(\rho c)_1} t_{12}^2$$

where $\rho$ and $c$ are the density and speed of sound in the respective media.

Under the experimental conditions $\rho_g = 0.18$ lb per ft$^3$, $c_g = 3100$ ft per sec, and $\rho_s = 100$ lb per ft$^3$. A $c_s = 1000$ ft per sec was assumed. The calculated amplitude ratio is 0.01 and the energy ratio is 0.02. Extensive changes in $c_s$ will not affect the magnitude of the calculated amplitude and energy ratios. The gauges were calibrated low in the first run because the calculation indicated that lower amplitudes were to be expected.

It was later realized that the amplitude in the propellant should build up until the gains and losses are balanced. If all other gains and losses are neglected except for the transmission into the gas, the solid-to-gas amplitude ratio is 0.075. Obviously, the oscillations in the gas cannot be of the order of 8000 psi peak-to-peak, although they may be from 2 to 4 times the value measured at the head-end.

The results indicate that the gas–solid acoustic interactions cannot be predicted on the basis of simple acoustic theory. The high pressure oscillations detected at the periphery cannot be explained. The effect of these higher than expected oscillations on the combustion-instability theory (Ref. 5) has not been examined.

### F. Propellant Variation

In order to study the effect on combustion instability of a small change in the oxidizer loading of the propellant, a modified formulation of Propellant A, called Propellant C, was prepared. The oxidizer loading was increased about 10%, and the other ingredients were reduced accordingly. The small amount of fiber contained in Propellant A was eliminated to improve castability. The increased oxidizer content gave a higher performance propellant with a $c^*$ of approximately 4500 ft per sec at 160°F. The burning rate at a given pressure was considerably increased, as shown in Fig. 21. The elongations at ultimate load obtained from tensile tests of this propellant were very low, except at 160°F where they were considered to be acceptable. Partly for this reason, all of the Propellant C firings have been conducted at a grain temperature of 160°F. Also, the main body of data from Propellant A firings were obtained at this grain temperature.

Figure 22 is a plot of high-frequency pressure amplitude, $P_{ac}$ versus $K_{n_i}$ for $3 \times 5 \times 31.0$ motors at a grain temperature of 160°F. The parameter $P_{ac}$ is the maximum value of oscillation amplitude on the Hathaway record observed during the initial period of instability and was chosen as near to the value of $P_{c_b}$ as possible. Mean-pressure data were not used to define instability level in this case because the severity of the oscillations combined with the poor propellant physical properties resulted in frequent grain break-up. This, in turn, caused unusually high pressure peaks, which were not reproducible, and caused a number of plugged mean-pressure gauges. Figure 22 shows that nearly the same trends are observed using this criterion of instability intensity as those which have been presented in the plots of instability level versus $K_{n_i}$ for Propellant A, except that the region of weak instability is not present and $K_{n_{max}}$ has been shifted to a much higher value.

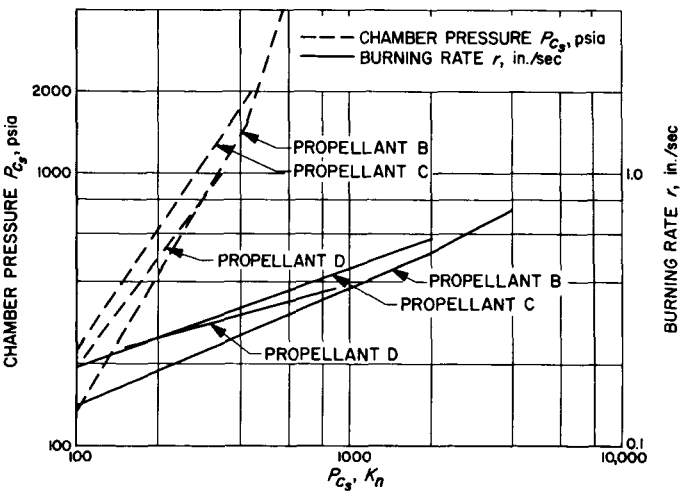


**Fig. 21. Burning-rate relations, Propellants B, C, and D**

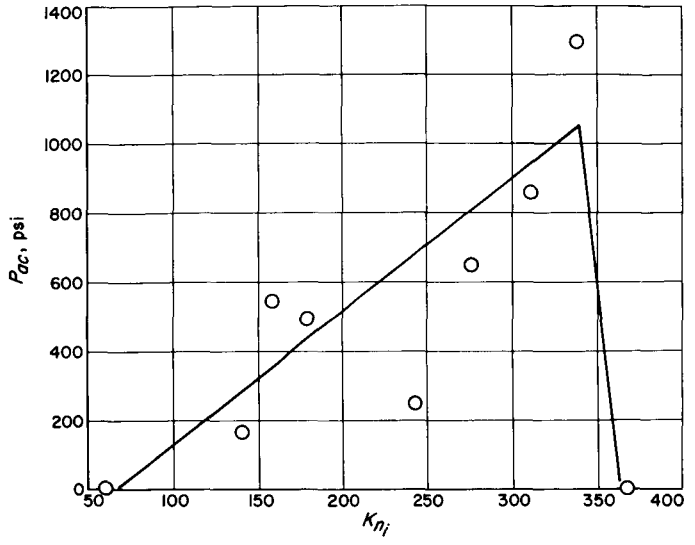


**Fig. 22. Oscillation amplitude vs $K_{n_i}$; Propellant C, motors 3 × 5 × 31 at 160°F**

Figure 23 is a plot of instability level versus $K_{n_i}$, defined in the usual manner. Because of previously mentioned difficulties with mean-pressure data, not all of the firings are included on this plot. The large values of instability level correspond to very large spikes on the pressure-time curve.

Figure 24 gives typical pressure-time curves for Propellant C firings; a low-pressure firing exhibiting low instability level and long delay time, a strongly unstable firing with a shorter delay time, and a completely stable firing. The low-pressure firing curve bears some resemblance to those curves shown in Fig. 14 for Propellant A. The pressure-time curve of the strongly unstable firing is quite similar to those curves which have been obtained from strongly unstable firings of Propellant A, except for the much shorter delay time, and, of course, the much higher average mean pressure. A comparison of these initial results for Propellant C with results for Propellant A support the idea that higher-energy propellants tend more toward instability than do lower-energy propellants.

Two other propellants, B and D, had less modification; Propellant B contained 1% of a moderate-burning-rate catalyst. The oxidizer grind was then modified to provide approximately the same burning rate-pressure relationship as Propellant A (Fig. 21). The 3 × 5 × 38 motors showed completely stable combustion when fired at pressures from 90 to 4250 psia at 160°F.

Propellant A was modified to Propellant D by adding 0.5% of 0.5-micron carbon black to the normal composition. Two 3 × 5 × 38 motors were fired at pressures just below and just above the pressure that would have resulted in maximum instability with Propellant A. Neither motor

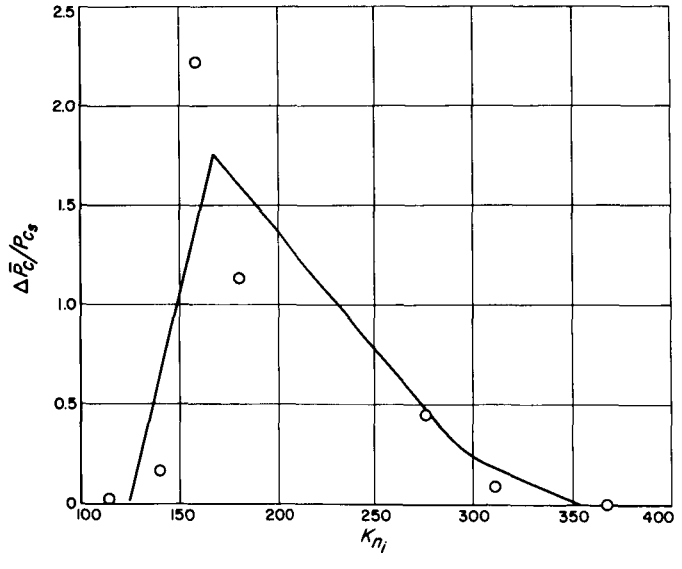


**Fig. 23. Instability level vs $K_{n_i}$; Propellant C, motors 3 × 5 × 31 at 160°F**

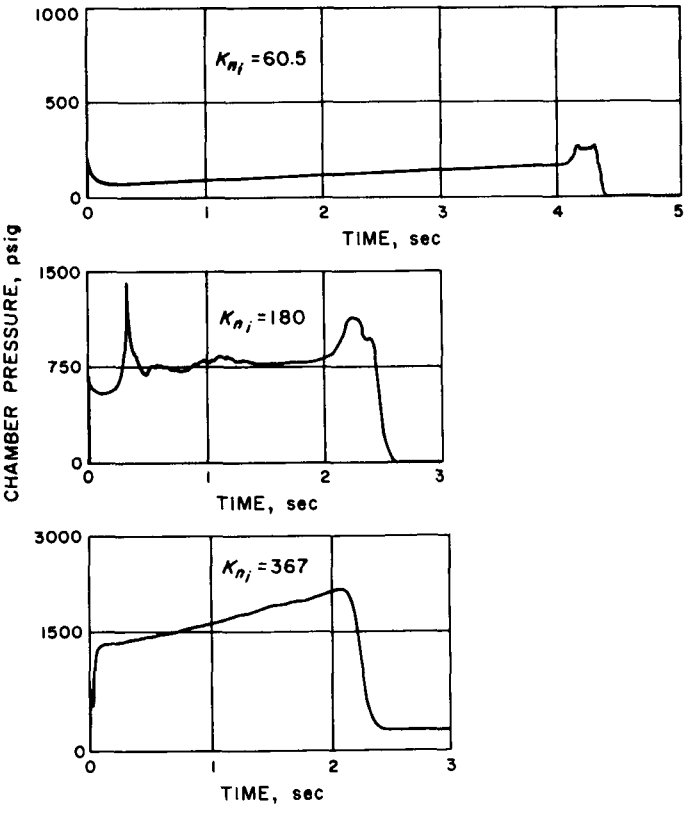


**Fig. 24. Typical Propellant C motor firings; 3 × 5 × 31 at 160°F**

showed pressure spikes or tangential oscillations. Both motors showed considerable longitudinal oscillations at a 50-psia peak-to-peak level, which is approximately twice the level normally found in Propellant A.

Recently, J. F. Bird (Ref. 6) indicated that, if the main damping mechanism is caused by smoke, the stability map (Fig. 19) could be qualitatively predicted by the Hart-McClure theory (Ref. 7). A quantitative fit was obtained for plausible smoke properties: 0.5% mass abundance, 0.5-micron radius. Presumably, increasing the fraction of smoke or small particles present would decrease the pressure range in which instability would occur. Thus, an explanation of the behavior of Propellants B and D is available, although it cannot yet be considered rigorous. A definitive experiment could be performed by adding only a sufficient amount of inert fine particles to alter the stability map. The complete elimination of instability could be caused by such other occurrences as a change in reaction time in a time-lag hypothesis. Unfortunately, it is difficult to obtain inert particles in the required size range. The possibility of performing a quantitative experiment should be considered.

### G. Head- and Nozzle-End Volumes

Several motors were fired to determine the effect of adding hollow chambers of various lengths to the head end or nozzle end of a motor which exhibited strong instability when fired without a hollow chamber. The motors used for this series of tests were all $3 \times 5 \times 38$ motors with throat diameters of 1.850 in. and grain temperatures of 80°F. The hollow chambers were made of Shelby tubing (as were the motor cases) and were attached to the motor cases with an adapter ring. Headplates or nozzleplates were attached to the opposite ends of the chambers. Holes were drilled and tapped into the adapter ring to permit the installation of two Photocon gauges at the same axial position on the motor and 90 deg apart on the circumference.

The chambers were lined with a polyurethane rubber to protect them from high temperatures. Slightly greater thicknesses of liner were consumed when the chambers were installed on the nozzle end than when they were installed on the head end because of the increased heat transfer caused by gas flow. In both instances, however, the burning-rate–pressure relationships and $c^*$ determined from reductions of mean-pressure data were only slightly affected by the liner pyrolysis.

Pressure-time curves from four firings of this series are presented in Fig. 25. Part A is from a motor without a head- or nozzle-end chamber. Part B shows a typical firing with a head-end chamber. Head-end void lengths of 8⅛, 11⅝, 13, 15⅝, 19, and 38 in. were used. One of the two firings made with a 13-in. void length was completely stable, and the firing at a void length of 11⅝-in. was moderately unstable; each of the other firings including the remaining one at 13 in. were strongly unstable, similar to the typical firing shown. Nozzle-end void lengths of 9⅜, 13, 19, 38⅜, and 73 in. were used. The motors fired with the shortest voids were completely stable. Faint instability was detected in the motor with the 19 in. void, and instability increased slightly with void length for the remaining two firings. Results of two typical firings are shown in Fig. 25.

The effect of these hollow chambers does not appear to be one of eliminating specific frequencies which bear a fixed relationship to some natural frequency of the chamber. The frequency of the first tangential of the port, as it increases from 3 to 5 in., decreases by more than one-third of its initial value. If the change in instability were related to an acoustic frequency of the void, the effect of a nozzle-end void should also be observed if instability were attenuated by damping of the plenum-chamber variety. If this were the case, the attenuation should increase with chamber volume and effect exactly the opposite of that which is observed in the case of the nozzle-end chambers.

Frequency analyses were performed upon the tape-recorded outputs from the Photocon gauges obtained from several of the motor firings which employed head-end and nozzle-end chambers. No frequencies were observed which could be identified positively as longitudinal modes of either the grain perforation or the hollow chamber. Earlier data from this research program have indicated that the first longitudinal mode of the port has been present at low amplitudes during nearly all firings, regardless of the presence or absence of the first tangential mode. It appears that combustion instability in these motors associated with the first tangential mode is independent of the presence or absence of the first longitudinal mode.

### H. Torque Produced by Combustion Instability

Motors which exhibited severe combustion instability were often found to have rotated about the longitudinal axis during the firing, even though they were restrained by three heavy chains which were tightened across the motor cases. The motor cases were held by the chains against V-blocks which rested against the test stand.

It is believed that the torques were caused by gas rotation in the port. If this were the case, an expression

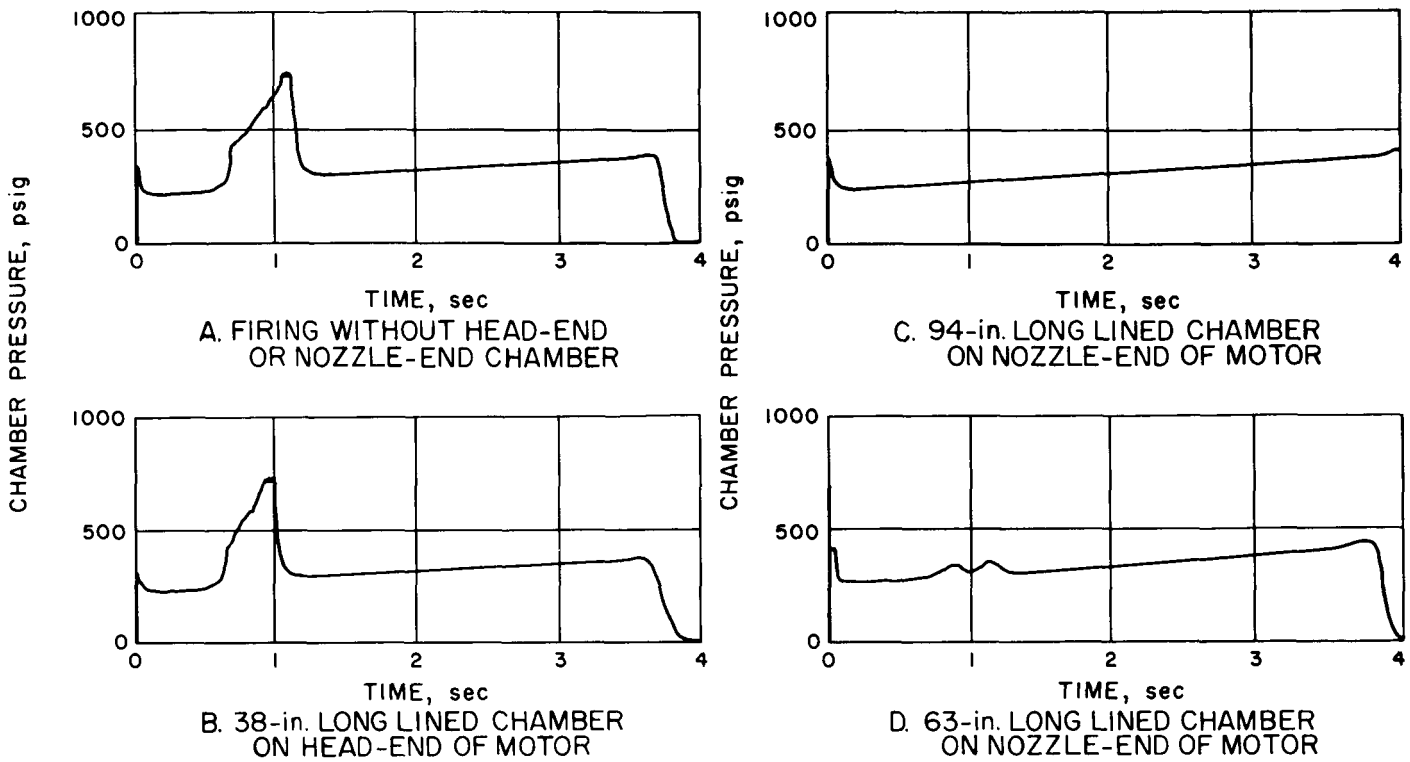


**Fig. 25. Effect of head- and nozzle-end chambers on instability; motors 3 × 5 × 38 at 80°F, $K_{n_i} = 135$**

for torque can be written in terms of a shear stress between the gas and the propellant burning surface,

$$\theta = \tau A_b D_p/2 \tag{3}$$

where $\theta$ is the torque, $\tau$ is the shear stress, $A_b$ is the propellant burning area, and $D_p$ is the port diameter. This equation neglects the nozzle-end and head-end effects and considers an average shear stress over the entire burning surface. It is possible to write the shear stress in the form

$$\tau = C_D \tfrac{1}{2} \rho_g U_\theta^2 \tag{4}$$

where $C_D$ is a drag coefficient between the gas in the port and the propellant burning surface, $\rho_g$ is an average gas density, and $U_\theta$ is the velocity component parallel to the propellant surface and normal to the longitudinal motor axis. Combining Eqs. (3) and (4),

$$U_\theta = \frac{2}{D_p}\left(\frac{\theta}{\pi C_D L \rho_g}\right)^{1/2} \tag{5}$$

where $L$ is grain length.

A typical value of $U_\theta$ was calculated, with $D_p = 4$ in., $L = 40$ in. and $\rho_g = 3 \times 10^{-4}$ lb per in.$^3$ This is the density which is calculated for products of Propellant A at a pressure of 800 psia. The value of $\theta$ was assumed to be 600 lb-ft, an estimate obtained from the torque required to turn a motor in the stand with a strap wrench. It was believed that the drag coefficient for gas flow parallel to a transpiring surface must be quite low, and a value of 0.05 was assumed. The calculated value of $U_\theta$ for this case was 1600 ft per sec. Although this calculation is a crude approximation, the order-of-magnitude of the results indicate that the mechanism which was assumed is probably reasonable.

The existence of these rather large torques which accompany severe combustion instability suggests that smaller torques may exist when oscillation amplitudes are low. If this is the case, the use of resonance "fixes" which merely reduce the oscillation amplitudes to values which seem to be acceptable in static tests may not be satisfactory for flight applications.

### I. Erosive-Burning Mechanism

The mean-pressure–time curve could be used to obtain burning-rate–pressure data. The correct mass-balance equation for a solid-propellant rocket motor is

$$rA_b\rho_s = \frac{MV}{RT}\frac{dP}{dt} + \frac{gA_t P}{c^*} \tag{6}$$

Normally the term containing $dP/dt$ is neglected, although this could amount to an error of about 15% in the highly unstable firings. Calculations made in the reduction of data discussed in this Section did not neglect the $dP/dt$ term.

The experimental data can be reduced in order to obtain burning-rate increase as a function of ac pressure oscillations. The apparent burning-rate increment during the declining portion of the pressure spike is usually much higher than it is during the increasing portion. This is readily understandable as the instabilities through surface crazing and grain damage cause an increased burning area than cannot be accounted for in the data reduction.

The burning-rate increases before the "break" point, however, show reasonable agreement as indicated in Fig. 26, which presents data from a number of 3 × 5 × 31 motors fired at 160°F with $K_{n_i} = 130$. Only data obtained with heavy head plates have been reduced thus far because it is believed that the accelerations in the light head plates would have too great an effect on $P_{ac}$ data. The data from two high-frequency gauges were combined to obtain the correct peak-to-peak amplitude. No correction was made for the difference in radius between gauge and propellant. The burning-rate increment plotted in Fig. 26 is the fractional increase over that expected at that pressure; that is,

$$\frac{\Delta r}{\bar{r}} = \frac{r - r(\bar{P}_c)}{r(\bar{P}_c)} \tag{7}$$

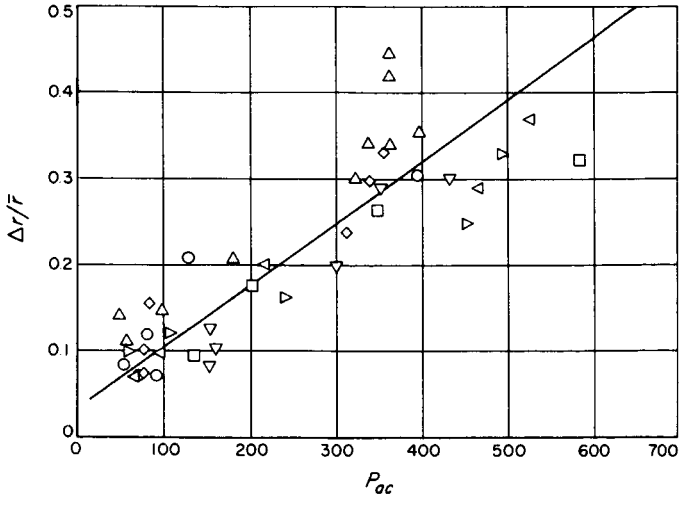


**Fig. 26. Burning-rate increment vs oscillation amplitude; motors 3 × 5 × 31 at 160°F, $K_{n_i} = 130$**

An early study of the erosive burning properties of this propellant yielded

$$r = aP^n(1 + b_1 G) \tag{8}$$

where the units of $G$ are lb per in.$^2$ sec, and

$$\frac{\Delta r}{\bar{r}} = b_1 G = 0.2G \tag{9}$$

The ac pressure oscillations are proportional to $G$ as follows: The maximum acoustic particle velocity at the propellant surface is

$$\bar{U}_{\max} = \frac{c}{2\alpha_{mn}\gamma\pi}\frac{P_{ac}}{c} \tag{10}$$

where the difference between gauge placement and surface is neglected. The average velocity during one cycle is, considering only absolute values,

$$\bar{U} = \frac{2}{\pi}U_{\max} \tag{11}$$

and

$$G = \rho\bar{U} = \frac{g P_{ac}}{c\,\alpha_{mn}\pi^2} = 0.0018\,P_{ac} \tag{12}$$

The line drawn in Fig. 26 gives

$$\frac{\Delta r}{\bar{r}} = b_2 G = 0.4G \tag{13}$$

The disagreement between the constants in Eqs. (9) and (13) gives little credence to the erosive-burning concept; however, there are other factors to be considered.

A more recent theoretical treatment of erosive burning by Lenoir and Robillard (Ref. 8) gave the following:

$$r = aP^n + \frac{\alpha_c G^{0.8}}{L^{0.2}} e^{-\beta r\rho_s/G} \tag{14}$$

where $\alpha_c = 2.25 \times 10^{-4}$ ft$^{2.8}$ per lb$^{0.8}$ sec$^{0.2}$, approximately the same for all propellants and $\beta = 53$ for this propellant. Equation (14) is somewhat complicated for use in the present situation; however, note that $\alpha_c$ and $b_1$ of Eq. (6) should be related. The development of Eq. (11) was based on a heat-transfer theory, and $\alpha_c$ is proportional to the flat-plate turbulent-boundary-layer heat-transfer coefficient.

Morrell (Ref. 9) has presented a theory and has discussed some experiments on the ratio of heat transfer

during oscillating flow to that under steady flow. For a steady-state Mach number of 0.1, in terms of our variable, the heat-transfer ratio $R_0$ is, very approximately,

$$R_0 = \frac{2 P_{ac}}{P_c} \tag{15}$$

The average Mach number down the grain of these motors is about 0.075; therefore, the increase in heat transfer should be greater (see Ref. 4). The range of $P_{ac}$ in Fig. 26 corresponds to a range of $P_{ac}/P_c$ from 0 to 1.0. The ratio of $b_2/b_1 = 2$ is, therefore, entirely reasonable. The concept that an erosive burning mechanism causes the increased burning rates appears reasonable.

Values of $U$ computed from Eq. (11) for the data points on Fig. 26 are approximately the same, or less, than an axial gas velocity based upon an average Mach number of 0.075. However, during the portion of the run before the onset of instability, these motors did not exhibit a measurable burning-rate increment which could be attributed to erosive burning. Because the axial gas velocity apparently did not contribute a burning-rate increment, it was not considered further.

This evidence also indicates that, if an erosive-burning mechanism is responsible for the increased burning rate during periods of instability, either the coefficient "$b_1$" in Eq (8) should be very different in the oscillatory case from its value in the quasi-steady-state case, or an entirely different expression should be used. Since the burning-rate increment is approximately proportional to the peak-to-peak pressure amplitude, the form of Eq. (8) seems reasonable.

## IV. SUMMARY

Experimental results have shown that the delay time from ignition to onset of instability might be correlated with propellant physical properties, but the negligible effect upon delay time of pressurizing a motor prior to firing indicated that the time required for the grain to approach an equilibrium strain condition was probably not connected with delay time. Nor did a reduction in heat loss to inert motor parts show any effect on delay time, and this phenomenon is still unexplained.

In Ref. 1, it was demonstrated that a motor firing with a particular grain geometry and grain temperature would exhibit increasingly severe instability, then a sudden change to weak instability, and finally stable operation as chamber pressure was increased. These trends were also found to exist for a wide range of grain temperatures and for several different sets of grain dimensions. Regions of strong instability, weak instability, and stable operation were outlined in the pressure-frequency and the pressure-grain temperature planes for several grain geometries. Firings of motors at chamber pressures below 100 psia indicated that a low-pressure region of stability might exist.

It has been demonstrated that a critical grain length, or $L/D$, is required if severe instability is to occur. For motors longer than the critical, length did not affect instability level. The critical length was shown to be affected by grain temperature and material lot variations.

Results from motor firings with different grain thickness and different grain temperatures with the same web thickness indicated that propellant physical properties

and web thickness affect unstable combustion significantly. An unstable motor firing in which pressure was measured at the interface between the propellant and the motor case showed pressure waves which were strongly transmitted through the propellant. The results indicate that the gas-solid interaction cannot be predicted on the basis of simple acoustic theory.

Three modified forms of Propellant A were prepared. Two in which additional fine particles were present exhibited stable operation. Another modification in which the oxidizer loading was increased showed nearly the same trends with respect to plots of instability level versus $K_n$ which were shown by Propellant A, but this higher-performance modification was strongly unstable over a much wider pressure range.

Results from motors which were fired with hollow head-end and nozzle-end chambers of various lengths demonstrated that the effects of these chambers upon unstable combustion were neither of damping selective frequencies, or purely viscous-damping effects. Longitudinal modes were not detected in any of these firings. Since longitudinal mode frequencies were detected in most of the earlier firings, it was concluded that combustion instability associated with the fundamental tangential mode is independent of the longitudinal mode.

It was noted that motors which were strongly unstable tended to rotate in the test stand during the firing. This was assumed to be caused by rotating gas flow in the port. The magnitude of the angular velocity was estimated.

Correlation of high-frequency pressure amplitudes with burning rate increments strongly supports the contention that the increased burning rates observed during combustion instability can be attributed to an erosive-burning mechanism.

## NOMENCLATURE

| | |
|---|---|
| $a$ | burning-rate constant in $r = aP^n$ |
| $A_b$ | area of burning surface |
| $A_t$ | nozzle throat area |
| $c$ | local velocity of sound, ft/sec |
| $c^*$ | propellant characteristic velocity, ft/sec |
| $C_D$ | drag coefficient, propellant-gas interface |
| $d_t$ | diameter of nozzle throat, in. |
| $D_p$ | diameter of grain perforation, in. |
| $G$ | mass velocity, lb/in.$^2$ sec |
| $I$ | acoustic intensity ratio |
| $K_n$ | ratio of burning area to throat area |
| $K_{n_{max}}$ | $K_n$ leading to maximum instability |
| $K_{n_s}$ | $K_n$ leading to stable run |
| $L$ | length |
| $M$ | molecular weight of combustion gases |
| $n$ | burning rate exponent in $r = aP^n$ |
| $P$ | pressure, psia |
| $P_{ac}$ | peak-to-peak pressure oscillation, psi |
| $\bar{P}_c$ | mean chamber pressure, psia |
| $\Delta\bar{P}_c$ | increase in mean chamber pressure caused by instability, psia |
| $\bar{P}_{c_B}$ | mean pressure at "break" point, psia |
| $P_{c_s}$ | normal expected stable pressure, psia |
| $r$ | burning rate, in./sec |

## NOMENCLATURE (Cont'd)

$\Delta r$ increase in burning rate, in./sec

$r$ normal burning rate at $P_c$, in./sec

$R$ universal gas constant

$t$ time, sec

$t_{12}$ amplitude ratio

$T$ temperature

$U_\theta$ tangential gas velocity normal to the motor's longitudinal axis

$V$ volume occupied by propellant combustion products inside motor

$\alpha_{mn}$ mode number

$\gamma$ specific heat ratio

$\theta$ torque

$\rho$ density, lb/in.$^3$

$\tau$ shear stress at propellant-gas interface

Subscripts

$g$ gas-phase property

$i$ at ignition

$p$ port or propellant

$s$ solid-phase property

## REFERENCES


1. Brownlee, W. G., *An Experimental Investigation of Unstable Combustion in Solid-Propellant Rocket Motors*, Memorandum No. 20-187, Part I. Jet Propulsion Laboratory, Pasadena, California, December 30, 1959.
2. Brownlee, W. G., and Marble, F. E., "An Experimental Investigation of Unstable Combustion in Solid Propellant Rocket Motors," *Solid Propellant Rocket Research* (pp. 455–494), Academic Press, New York, 1960.
3. Landsbaum, E. M., Kuby, W. C., and Spaid, F. W., "Experimental Investigations of Unstable Burning Solid Propellant Rocket Motors," *Solid Propellant Rocket Research* (pp. 495–525), Academic Press, New York, 1960.
4. Spaid, F. W., and Landsbaum, E. M., "Instrumentation for Research on Combustion Instability in Solid-Propellant Rocket Motors," *Liquid Rockets and Propellants* (pp. 119–143), Academic Press, New York, 1960.
5. Wood, A. B., *A Textbook of Sound* (pp. 301–304), G. Bell and Sons, Limited, London, 1955.
6. Bird, J. F., McClure, F. T., and Hart, R. W., *Acoustic Instability in the Transverse Modes of Solid-Propellant Rockets*, TG-335-8. Applied Physics Laboratory, Silver Spring, Maryland, June 1961.
7. Hart, R. W., and McClure, F. T., "Combustion Instability Acoustic Interaction With a Burning Propellant Surface," *Journal of Chemical Physics*, 30(6): 1501–1514, June 1959.
8. Lenoir, J. M., and Robillard, G., "A Mathematical Method to Predict the Effects of Erosive Burning in Solid Propellant Rockets," *Sixth Symposium on Combustion*, (pp. 663–667), Reinhold Publishing Corporation, New York, 1956.
9. Morrell, G., "An Empirical Method for Calculating Heat Transfer Rates in Resonating Gaseous Pipe Flow," *Jet Propulsion*, Technical Note, 38(12): 829–831, 1958.